Measurement setup to simultaneously explore the location and energy of trapped charges in thin polymer films

Duvan Mendoza-Lopez, Laurent Berquez, Laurent Boudou, Gilbert Teyssedre

Measurement Setup to Simultaneously Explore the Location and Energy of Trapped Charges in Thin Polymer Films

Duvan Mendoza-Lopez[a)], Laurent Berquez, Laurent Boudou and Gilbert Teyssedre

LAPLACE, Université de Toulouse, CNRS, INPT, UPS, Toulouse, France
118 route de Narbonne, F-31062 Toulouse cedex 9, France

[a)] Corresponding author: mendoza@laplace.univ-tlse.fr

Abstract. This research work proposes a unique system that combines charge density measurements by the laser intensity modulation method (LIMM) with optically excited current acquisitions using the photo-stimulated discharge technique (PSD). The purpose of this setup is to investigate the relationship between space charge properties (such as density, spatial depth, and time evolution) and the photocurrent-associated energies in order to gain new insights into the trap population and detrapping mechanisms in thin polymer films. This paper presents a description of the technical principles of both methods as well as the whole combined system. The results on a 12 µm-thick polyethylene naphthalate (PEN) film show pyroelectric currents which, after processing, indicate the formation of homocharges whose magnitude and depth decrease after light irradiation. The PSD currents allow the identification of two major energy bands at 3.4 eV and 5.9 eV (360 nm and 207 nm, respectively), possibly related to charge detrapping. In addition, current transients during constant wavelength irradiation show that incident photons can interact differently with trapped charges depending on the applied field.

INTRODUCTION

Polymer dielectrics play a crucial role in energy storage and conversion devices. Their ability to accumulate electrostatic energy, as well as their dielectric properties make them widely used in film capacitors[1–3] and electrical insulation applications such as cables or electronic components[4,5]. The constant search for better performance and long lifetimes makes it necessary to characterize their electrical behavior based on charge carrier dynamics.

Charge generation inside a dielectric material subjected to a high electric field can be explained by the injection of charges from the electrodes, the generation of ionic species, or donor state phenomena[6]. Microscopic approaches complementarily suggest that these charges can be trapped in structural or chemical defects, which are energetically related to localized states ranging from shallow (0.1-1 eV) to deep (>1 eV) traps[7]. Space charge is then defined as the set of charges that accumulate at these trapping sites and whose density can modify the internal electric field, resulting in electromechanical forces that may promote electric breakdown[8]. The study of space charge and trapping/detrapping phenomena in polymer films is then necessary to understand and improve their reliability for industrial applications.

Numerous non-destructive space charge measurement methods, that focus on the amount and spatial location of charges within the material[9], have been developed for different insulation configuration including both cylindrical and flat specimens. For flat and thin samples, the LIMM (*Laser Intensity Modulation Method*) is a suitable option since its resolution has been reported to be as low as 1 µm near the electrode where the thermal perturbation is applied[10]. For example, LIMM acquisitions on polyethylene naphthalate (PEN) samples show the formation of homocharges by carrier injection[11,12]. These studies do not usually include information to identify the energetic nature of the traps and it is by applying techniques such as TSDC (*Thermally Stimulated Discharge Current*), PSD (*Photo Stimulated Discharge*), or TL (*Thermo Luminescence*) that the energetic states of charge release and recombination can be explored[13]. Some TSDC and TL experiments on PEN have determined activation energies in the range of 0.1-0.7 eV and suggest that they are related to both detrapping phenomena and molecular motions[14,15]. Other works using optical perturbations reported trapping depths of 4.1 eV for PET (polyethylene terephthalate) from PSD currents analysis[16]. However, few publications have been published on configurations to identify the location, density and trapping depth

of the space charge in the same measurement bench. Preliminary results from a combined LIMM-PSD system in BOPP have been reported showing possible relationships between the decrease in charge density and photocurrent peaks corresponding to energies of 3.2 eV and 6.2 eV[17,18].

This paper presents the technical details of a test bench combining LIMM and PSD techniques and some typical results obtained on a 12 μm PEN sample. The in-depth charge density evolution is monitored when traps are populated by a DC electric field and perturbed with light irradiation that promote charge detrapping. Initially, the two methods are described with particular attention to the relationship between thermal and optical excitation with outgoing low-intensity currents. Then, full system features and its implementation are shown. Space charge densities and PSD results are finally presented, with emphasis on the current spectra evolution showing consistency of the results.

MEASUREMENT TECHNIQUES AND DETAILS

LIMM Principles

In the early 80s, Lang et al. presented the frequency-based LIMM method as an alternative to the time domain technique TPM (*Thermal Pulse Method*) for the study of polarization and space charge in polymer insulators. The TPM system needed high technological requirements and the LIMM procedure was able to provide higher accuracy using conventional equipment[19]. Since then, both techniques have evolved making TPM a method with shorter acquisition times while LIMM signal processing and interpretation is less demanding[20].

The operating principle of the LIMM is shown in Fig. 1. This method employs a frequency-modulated laser that heats the metallic electrode of an insulating film and produces inhomogeneous thermal waves diffusing in the bulk. These temperature variations lead to material expansion and changes in the local dielectric permittivity that affect the orientation of the dipoles. The weak displacements of the charges in respect to their initial positions result in a rebalancing of the influence charge density at the electrodes[10]. In response, a pyroelectric current depending on the modulation frequency is measured in the external circuit, amplified (due to its amplitude of a few pico-Amperes), and treated to recreate the polarization or charge profile as a function of the distance from the electrode.

The pyroelectric current density *J(f)* reflects the variation of the spontaneous polarization of the material as a function of its thermal energy[21]. Therefore, the expression of the LIMM current *I(f)* will depend on the distribution of the temperature *T(z,f)* and a charge function *r(z)* that gathers the contributions of space charge as follows:

$$I(f) = \int_S J(f)dS = j2\pi f \frac{S}{L}\int_0^L r(z)T(z,f)dz \quad (1)$$

where *S* is the contact area between the laser and the electrode, *L* is the sample thickness and:

$$r(z) = p(z) - (\alpha_z - \alpha_\varepsilon)\varepsilon E(z) \quad (2)$$

where *p(z)* is the pyroelectric coefficient for polar samples, α_z and α_ε are the coefficients of temperature dependence of the thickness and the permittivity respectively, ε is the sample dielectric permittivity, and *E(z)* is the electric field.

The determination of *r(z)* from the current *I(f)* requires the definition of the temperature at each frequency and each depth of the material. Since direct measurement of the temperature inside the material is almost impossible, this study employs a calculation of the heat diffusion inside the insulator using a one-dimensional 6-layer thermal model[22]. In this multilayer approach, it is possible to access to the temperature evolution through the system by considering the incident and reflected light fluxes, the temperature continuity conditions, and the heat flux for each interface.

Once the LIMM current is measured and the temperature parameters of the system are calculated, the *r(z)* distribution can be established by applying a deconvolution technique to equation (1) (whose form represents a Fredholm integral equation of the first kind). This mathematical treatment is often tricky because it deals with experimental current signals that may produce unstable solutions. The Tikhonov regularization method implemented in this study proves to be reliable for calculating the space charge density profile[23]. After reconstructing the charge distribution *r(z)*, the electric field profile *E(z)* can be obtained and confirmed by a thermal model calibration procedure[24]. The space charge distribution can then be determined from the derivative of the electric field.

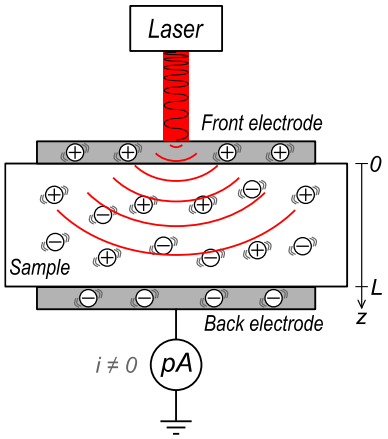

FIGURE 1. Principle of the LIMM method. When a laser beam heats the front electrode of a metallized sample, thermal waves are generated and the intrinsic charges are perturbed. The redistribution of charges at the electrodes creates a pyroelectric current.

PSD Principles

Historically, the study of electrical conduction in semiconductors and insulators has been based on determining the energy-band model of the material, and in particular the trapping states in the band gap. The idea was to develop methods in which an energetic perturbation, optical or thermal, can excite these traps, whether they are deep or not. One of them is the PSD method first published by Brodribb et al. in 1972[25]. It is based on the optical excitation of the sample at particular photon energies for the measurement of a current response related to that energy.

In this technique, a sample is irradiated with monochromatic light while following the external short-circuit current as a function of the wavelength from infrared to UV spectrum. The insulating material can be previously charged or not to a constant temperature (under conditions preventing as much as possible variations of the stored charge such as release by thermal excitation). The measured photocurrents can then be explained by one or more of the following phenomena[26] (illustrated in Fig. 2): photoemission effects where carriers are injected from the excited electrode to the insulator or electrons are emitted from the dielectric to the bottom electrode; photocarrier generation when excitons (electron-hole pairs) are dissociated and interact with trapped charges or impurities; direct photoexcitation of carriers (trapped or not) jumping to the conduction or valence band. Whichever the process, charge motion is necessary to create an external current. Although light can pass through the metal electrode, a greater current amplitude is obtained by leaving areas of the polymer uncovered. This signal enhancement is explained by greater light penetration in the dielectric by avoiding light absorption and reflection by the metal.

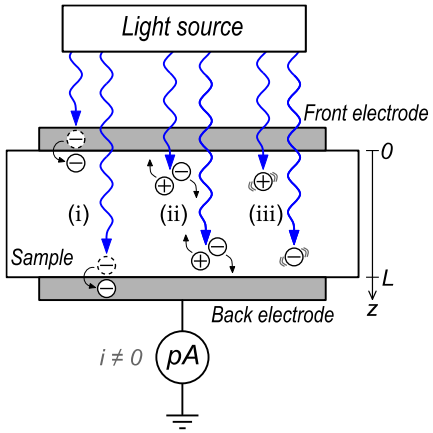

FIGURE 2. Principle of the PSD method. The external current during light exposure can be explained by photoemission phenomena (i), photocarrier generation (ii), and/or direct photoexcitation of carriers (iii).

Coupled Measuring Setup

This research is based on the coupling of LIMM and PSD measurements in a unique setup that allows consecutive tests without having to manipulate the sample, the test cell or the wiring connections. As the measurement system does not need to be handled, electrical charge conditions are not affected by external contacts or time lapse while changing methods. This also allows optimization of the experimental time. The main objective is to be able to study the evolution of the in-depth charge density while light irradiations promote charge de-trapping. As a result, not only space charge formation may be monitored but trap population and de-trapping scenarios can be investigated.

The system focuses on a controlled switch that allows the selection between the LIMM and the PSD sensing circuits. The mechanism consists of a magnetically actuated changeover reed switch which connects one of the measuring circuits (depending on the position of the magnet) to the output of the test cell. This provides complete galvanic isolation between the measurement and control circuits. As the two methods are based on the acquisition of very low current signals, it is important to reduce any electrostatic and electromagnetic interference. As a first preventive action, a shielding system is implemented to the cabling and the switching device. In the latter, through which the different measured signals flow, the suggested shielding is a metal box that encloses the reed switch circuit and has a connection to the ground[27]. Attention is also paid to limiting the ground loop currents and electrical noise interference by connecting only one instrument to the power line ground, as recommended in the operating manuals[28].

A schematic of the experimental setup developed for this study is shown in Fig. 3. The test cell is designed to accommodate circular samples of thin polymer films with a diameter of 8 cm. On each face of the film, 50 nm thick gold electrodes are deposited by the sputtering method. The front electrode has a particular shape as shown in Fig. 3 (a): this electrode leaves certain areas of the polymer uncovered, enhancing the penetration of the incident light into the sample during PSD measurements. The back electrode is a circular layer of 4 cm in diameter. The charging process is ensured by a high-voltage DC (HVDC) source connected to the front electrode through an RC filter that limits the leakage current and conditions the input signal.

The following LIMM setup characteristics have been extensively detailed in previous research[24]. This part of the coupled system is composed of a laser diode (PMT100, 100 mW, 660 nm) which is modulated in the frequency range from 10 Hz to 10 kHz. The spot diameter on one of the metallic slots is ~2 mm. The signal measured in LIMM mode travels from the back electrode to the electrical protection through the switch. The role of this protection circuit is to limit any breakdown overcurrent and may act as a low-pass filter with an approximately cut-off frequency of 10 kHz[24]. The measured current is pre-amplified by a low noise current amplifier (FEMTO LCA-200k-20M, bandwidth 200 kHz, gain 20 MV/A), then a lock-in amplifier (SIGNAL RECOVERY Model 5210) recovers the signal suppressing the effect of noise and decomposes it into the real and imaginary parts.

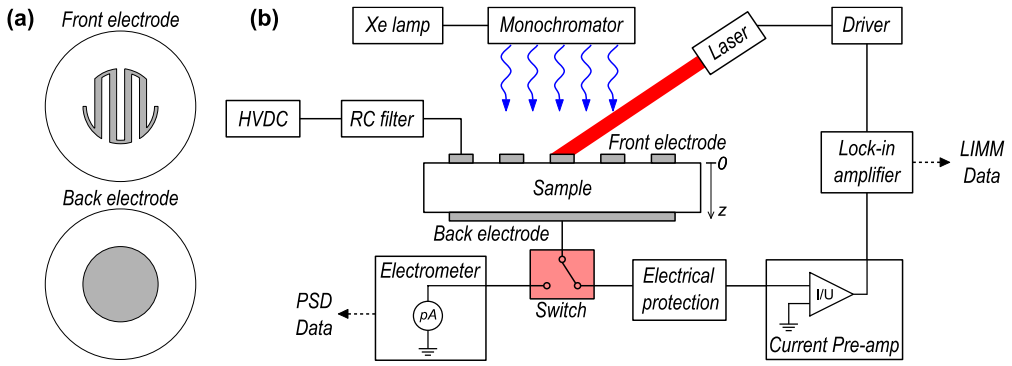

FIGURE 3. Schematic of a deposited electrode arrangement (a) and the LIMM-PSD coupled measurement setup (b).

Several factors determine the selection of the laser modulation frequency range. The primary consideration is the bandwidth of the measurement chain, which includes the electrical protection, preamplifier, lock-in amplifier, and driver. The second is the laser penetration depth δ_t, which decreases with increasing frequency following equation (3).

$$\delta_t = \sqrt{\frac{D_t}{\pi f}} \tag{3}$$

A $\delta_t \approx 2$ μm is calculated when polymeric materials are considered (thermal diffusivities D_t around 10^{-7} m^2/s) and a maximum frequency of 10 kHz is imposed by the electrical protection cut-off frequency. In order to obtain thermal disturbance in the depth of the sample, a minimum frequency of 10 Hz is set, which corresponds to $\delta_t \approx 80$ μm. The smallest distance from the front electrode that can be precisely represented in the resulting space charge profile[29], is estimated to be approximately 2 μm and may vary depending on the thermal diffusivity of the sample.

Concerning the PSD technique recently installed[18], the monochromatic light is produced by a 150 W Xenon short arc lamp (USHIO UXL-151H) associated with a 1200 gr/mm monochromator (Horiba Tunable PowerArc OB-2001). The entrance and exit slits are set to 2 mm to obtain a spectral bandwidth of typically 8 nm (wavelength dependent as shown in Table 1) which was measured with a spectrometer (Horiba HR4000-UV-NIR). While each spectrum contains mainly a fundamental peak that matches the imposed wavelength, there are also unfiltered harmonics whose amplitude is not negligible[18]. However, their contribution to the PSD current is not significant because the scan is performed from longer to shorter wavelengths.

TABLE 1. Light characteristics of the 150 W Xe arc lamp and the 1200 gr/mm monochromator at different wavelengths.

Fixed wavelength (nm)	Measured peak wavelength (nm)	Peak intensity (a.u.)	Peak width at half maximum (nm)
210	212	505	8
250	250	14593	8
300	300	6619	7
350	349	12679	8
400	398	12913	8
450	450	14397	8
510	509	14023	8
550	546	12277	8
600	598	8465	8

The incident irradiation is perpendicular to the surface of the sample and the irradiated area S is approximately 7 cm^2. Given these properties, Planck's constant h, the speed of light c, and using equation (4), it is possible to determine the number of photons incident on the sample in a given time η_{ph} by measuring the output power P as a function of the wavelength λ (using a thermopile sensor Newport 919P-00310).

$$\eta_{ph} = \frac{P \times \lambda}{h \times c \times S} \tag{4}$$

Figure 4 shows that the lamp has a higher photon flux density in the visible spectrum range and that as the wavelength reaches the UV spectrum the radiated photon flux decreases. The discharge currents are measured using an electrometer (Keithley 617) connected to the back electrode. Both the LIMM and PSD data are transmitted to a computer which performs the signal processing and drives the entire acquisition protocol using a Matlab application.

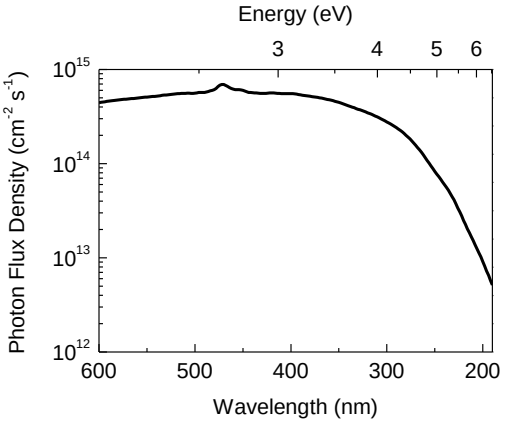

FIGURE 4. Photon flux density for the 150 W Xe arc lamp light source associated with a 1200 gr/mm monochromator.

Measurement program

To study the evolution of the charge density and the de-trapping phenomena in the sample, sequential measurement protocols are carried out as shown in the diagram in Fig. 5. Each row shows the applied method along with the number of times the action is repeated, its duration and the status of the high voltage source indicating whether or not the sample is subjected to an external electric field. *LIMM* tasks are laser-induced pyroelectric current acquisitions and have a duration of 10 minutes each to achieve the frequency scan. *PSD scans* are photocurrent spectrum recordings while the wavelength varies from low (2 eV, λ = 600 nm) to high energy (6.5 eV, λ = 190 nm) at a scanning speed of 24 nm/min. *PSD mono* refers to photocurrent acquisitions at a constant wavelength as a function of time.

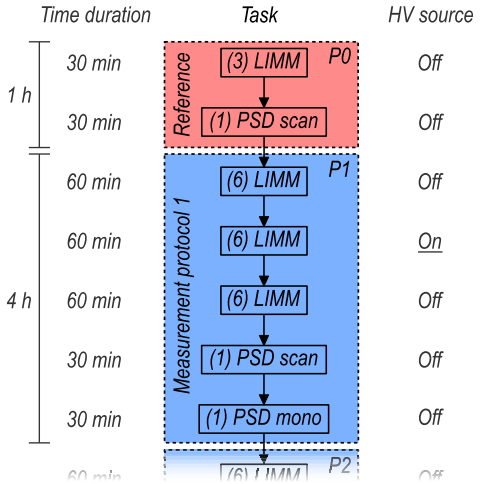

FIGURE 5. Measurement program of LIMM and PSD consecutive acquisitions.

This measurement program is mainly divided into two phases. The first one is called the *P0* reference phase and its objective is to measure the LIMM and PSD currents in the virgin sample , i.e., before any voltage application. It starts with three LIMM current measurements (for a total duration of 30 minutes) which are expected to be almost at zero pA since the sample has not been charged yet. However, *LIMM P0* acquisitions do contain non-zero currents that may be related to unfiltered electrical noise, induced charge migration during sample fabrication or permanent orientation polarization in the case of polar polymers. It is then important to identify the blank current from the average of the three reference measurements at zero volt and subtract it from the following LIMM acquisitions. As an example, Fig. 6 shows the average of the three non-charged LIMM reference measurements taken on a 12 µm-thick PEN sample. This figure shows that the blank current increases above 2 kHz, which is anomalous for a sample that has not been subjected to any charging period. When the average blank curves are subtracted from the rest of the measurements, the currents are representative of the sample charge conditions and generate consistent results when applying the deconvolution algorithm. The *PSD scan P0* completes the one-hour initial phase and serves as a reference to compare with subsequent measurements.

The second phase is a sequence of protocols *P1, P2... Pn* in which the sample is polarized with a specific voltage level in each cycle *Pi*. Each protocol involves the execution of several LIMM and PSD measurements as indicated in Fig. 5, each task with its own attributes. The *Pi* protocols consist of the following sequence of activities:

- Initial step at zero-volt, during which six LIMM measurements are executed, representing 1 h time.
- Polarization stage for 1 h, which involves the performance of six LIMM acquisitions.
- Voltage set at 0 V, allowing the execution of six LIMM recordings during the discharge phase.
  (The execution of six tasks per interval allows to identify the dynamics of the charging/discharging phenomena.)
- *PSD scan* from 600 nm to 200 nm.
- PSD acquisition at a fixed wavelength of 215 nm (*PSD mono*) to evaluate charge decay kinetics.
- Then LIMM measurement for *Pi+1* protocol starts immediately after the end of protocol *Pi*. This allows to follow the space charge variation before and after the sample is exposed to light irradiation.

As seen, the complete program allows the study of both trap filling and emptying processes by intercalating the two methods LIMM and PSD and varying characteristic parameters (supply voltage, polarity, steps duration, etc.).

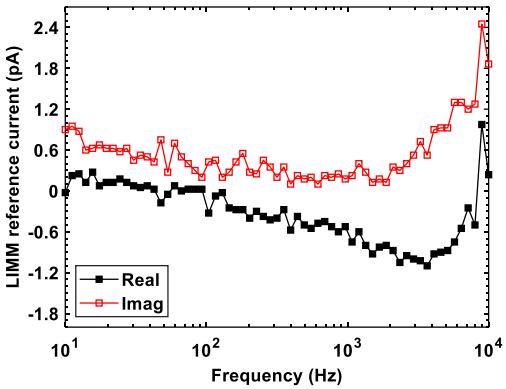

FIGURE 6. Average current for the 3 LIMM reference measurements on a 12 µm PEN sample.

Fig. 7 shows an example of the LIMM results obtained dynamically in a charging/discharging step. The real and imaginary parts of the current of each LIMM acquisition are measured in 10 min intervals on a 12 µm-thick PEN sample which has already been charged up to 80 kV/mm. The first measurements at zero volt show current values oscillating between -2 and 2 pA (Fig 7.a), representative of a previous charge step as the current is not zero. Every set of complex currents show similar features indicating almost no difference in the state of charge within this period. When an external field of 120 kV/mm is applied, currents of higher magnitude appear with a homogeneous behavior in all the recordings (Fig 7.b). After the charging step, the last interval at zero voltage shows the decay of the currents towards a stable position (Fig 7.c), with a reducing trend of the separation between the real and imaginary parts at high frequencies. When the charge state is stabilized, consecutive LIMM measurement show very similar current profiles reflecting a good repeatability of the measurements. When the charging state evolves in time, as during the discharge, the evolutions are continuous.

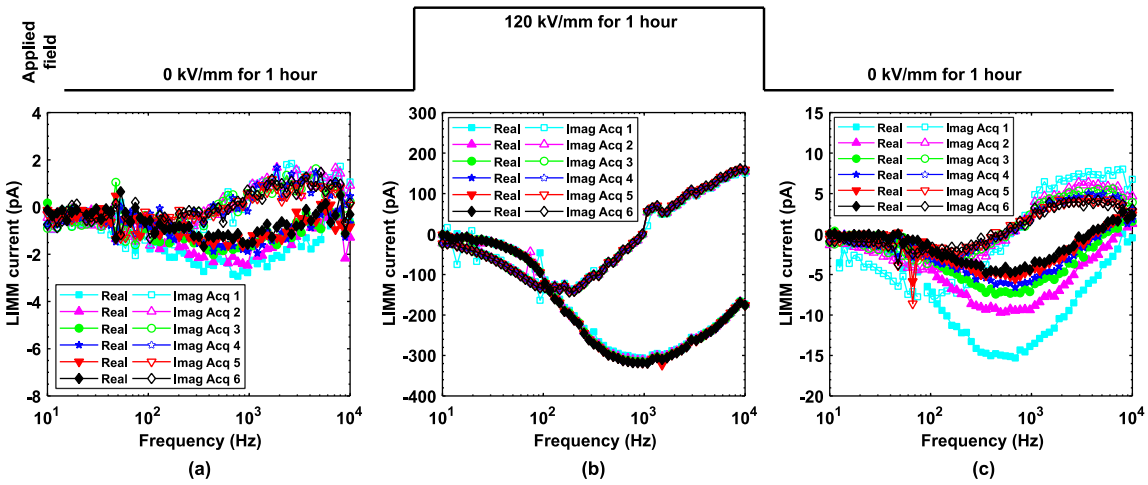

FIGURE 7. LIMM complex currents in three different intervals: before (a), during (b) and after (c) a polarization step of 120 kV/mm. Each period is composed of six LIMM acquisitions.

TYPICAL RESULTS

The results presented in the following were obtained under the electric field and light exposure protocol shown in Fig. 8, which in turn is based on the measurement program described in Fig. 5. This procedure is carried out on a 12 µm-thick PEN sample that has been prepared with the specifications outlined in the previous section. One sample was charged and discharged several times consecutively with positive polarization fields varying from 40 kV/mm up to 200 kV/mm by steps of 40 kV/mm. Note that, as written here, the field is positive when the voltage applied to the front electrode is positive. Progressive increase in electrical stress allows the analysis of carrier dynamics as traps are populated in the material. All experiments are performed at room temperature and atmospheric pressure.

The execution of this measurement program results in a substantial volume of data, considering the number of acquisitions made in each cycle. However, the aim of this publication is not to present a detailed analysis of every recording. Instead, the focus is to describe a configuration that combines the use of the LIMM and PSD methods, along with a demonstration of their validity and consistency through selected results. For this purpose, this study will concentrate mainly on the zero voltage intervals, as they provide insight into the charges that are trapped in the material. Furthermore, only one LIMM acquisition per interval will be presented, specifically the final recording in each zero-voltage period. This measurement provides information about the state of charge in a given cycle and can be used to show the evolution of space charge in successive polarization steps.

The results of the selected charge density measurements at the different pre-applied fields (LIMM0 to LIMM200) will be presented first to show the evolution of the charge accumulation. Next, the space charge behavior before and after the PSD200 measurement will be analyzed (LIMM200 and LIMM201). Finally, PSD spectra (PSD0 to PSD200) will be shown to study the photo-stimulated discharge phenomena.

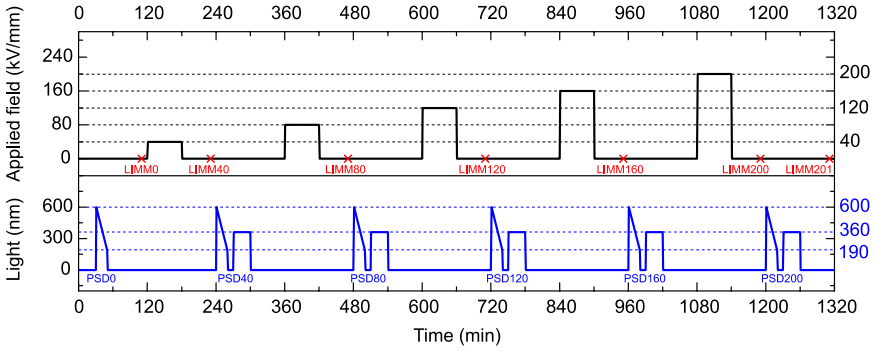

Figure 8. LIMM-PSD measurement protocol for positive polarization fields.

Evolution of the space charge density profiles

Figure 9 shows the measured LIMM currents along with the calculated charge density and residual electric field profiles one hour after the sample has been polarized (noting that the power supply is connected to the front electrode). In Fig. 9 (a) it can be seen that the magnitude of the LIMM current at low frequency is small (mostly close to zero) and that the real and imaginary components remain close to each other. For frequencies above 100 Hz, the current components begin to separate showing behaviors that depend on the applied field, i.e., a greater difference between components at higher field and smaller separation at lower field. Based on the inverse relationship between frequency and laser penetration depth as described in equation (3), the behavior of the currents indicates that at low frequencies the thermal waves penetrate deeper into the sample, but result in a relatively small perturbation, which may reduce the accuracy of the experimental data by a higher attenuation[30]. In contrast, higher frequencies result in a larger current signal that shows an increase in resolution as the irradiated electrode is approached.

The deconvolution process produces the residual electric field and space charge density profiles as shown in Fig. 9 (b) and (c), respectively. Upon visual inspection, it is apparent that there are well-defined patterns in both profiles, except for the region near the front electrode. The curves in this area exhibit unexpected fluctuations, which are likely due to inconsistencies in the electric field sampling points along the depth direction. In fact, in the PEN at a frequency of 10 kHz, the penetration depth of the thermal waves is reduced to 2.3 μm according to equation (3). For this upper frequency limit, the deconvolution and regularization methods are able to smooth a curve whose results are reliable from a depth of 1.5 μm. A zone of weak data precision is then defined from the electrode position down to the depth of 1.5 μm. To increase accuracy near the electrode, the modulation frequency of the laser and the overall bandwidth of the measurement chain should be increased, thereby reducing the depth of penetration into the material.

Figure 9 (b) illustrates the changes in the residual electric field as the sample undergoes the charging and discharging process with increasing stress levels. It can be observed that the electric field inside the sample shows transitions from being relatively uniform throughout the thickness to exhibiting gradually increasing slopes, ultimately reaching a peak value that is close to 5% of the pre-applied field. The negative field values near the front surface are a consequence of both the accumulation of charges, which modifies the field, and the numerical treatment that compensates the overshoot by altering the slope of the curve. The space charge density is obtained by calculating the derivative of the field functions and displayed in Fig. 9 (c). The results reveal that positive charges accumulate mainly

at a depth of 2 to 5 µm from the surface. It is clear that the amount of charge increases with the increasing electrical stress. The fluctuations near the positive electrode region are caused by changes in the compensating field.

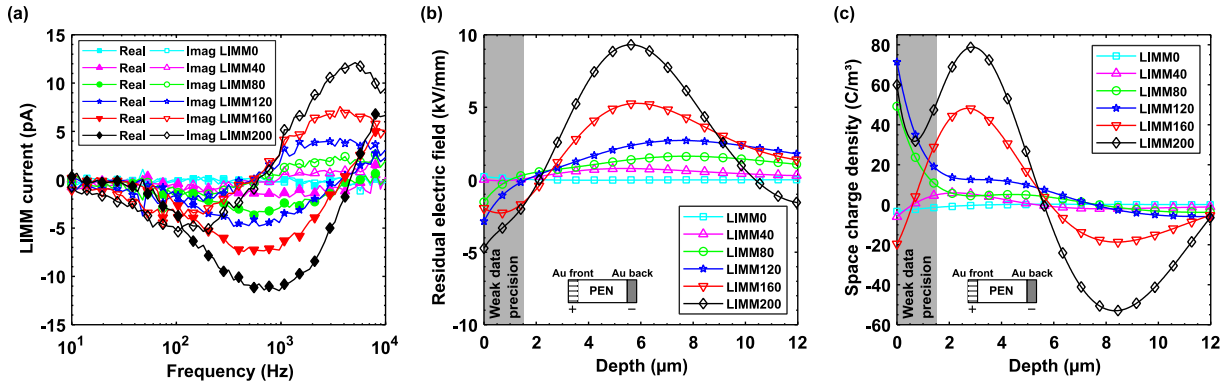

FIGURE 9. LIMM measurements on a 12-µm thick PEN sample after being polarized to different electric fields. LIMM complex currents (a), residual electric field (b), and space charge density (c). HV electrode to the left during polarization.

As described in Fig. 5, six space charge measurements are performed before and after each set of the PSD irradiations (scan and mono). This procedure is carried out systematically in order to compare the charge density just after polarization with that still present after photo-discharge.

Figure 10 presents the LIMM current, residual electric field and space charge density resulting from LIMM200 and LIMM201 measurements which are carried out before and after the PSD200 acquisition. Complex currents in Fig. 10 (a) illustrate how both the magnitude and the separation of their components are reduced once the PSD measurement is performed, i.e., in LIMM201 fewer charges are detected and less pyroelectric effect is revealed compared to LIMM200. There are at least two factors that can cause this effect: time and light irradiation. Consecutive LIMM recordings, such as those shown in Fig. 7, demonstrate the time effect as a smooth decrease in real and imaginary peak amplitudes while maintaining a similar shape, particularly at high frequencies. However, when comparing the LIMM behaviors before and after PSD measurements, it becomes evident that there are significant differences in the shape of the curves and a decrease in the current at maximal frequency (Fig. 10 a). These remarks suggest that light irradiation is at the origin of the decline of the LIMM signal, as a result of charge redistribution.

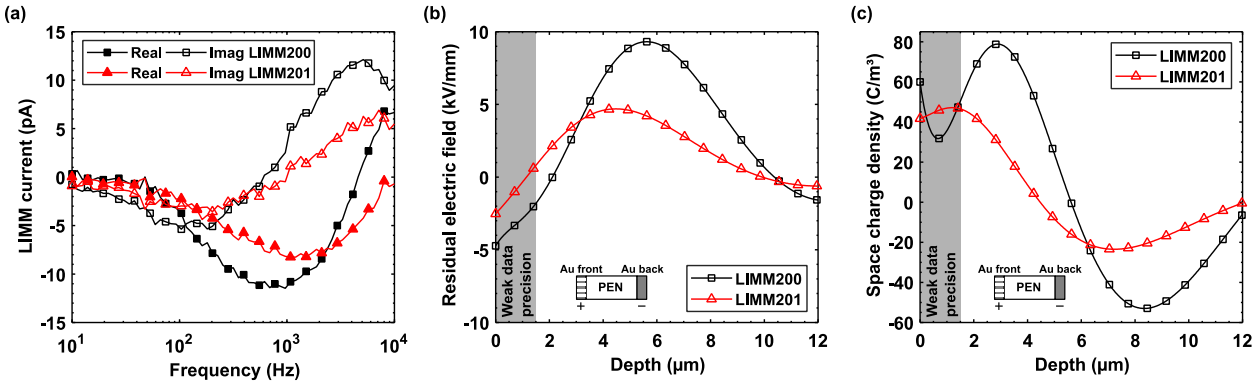

FIGURE 10. LIMM measurements on a 12-µm thick PEN sample pre-charged under 200 kV/mm. LIMM200 measurement is performed before PSD200 and LIMM201 after the same set of irradiations. LIMM complex currents (a), residual electric field (b), and space charge density (c). HV electrode to the left during polarization.

The processing of LIMM currents yields consistent results in terms of space charge and residual electric field. Figure 10 shows how the accumulated charge and the electric field near the front electrode are reduced after the sample has been irradiated. Although only the results from the last depolarization interval are presented, they are still valid when comparing the same position charge density profile before and after PSD recordings. Table 2 compares the

absolute integrated space charge density before and after PSD measurements for various levels of applied electric field. In every pair of compared values, the amount of accumulated charges is lower after light irradiation.

TABLE 2. Absolute integrated space charge density comparison before and after PSD measurements for several previously applied electric fields

Pre-applied electric field (kV/mm)	Absolute integrated charge density (C/m^3)	
	Before PSD	After PSD
40	28.3	2.0
80	74.5	26.7
120	131.5	41.8
160	239.8	119.2
200	507.5	254.9

Evolution of PSD currents

As one might expect, the current measured during photo-stimulation can come from different phenomena and not only from those related to light irradiation. In fact, the PSD curves initially lie on a decreasing baseline that may reveal the presence of long-lasting dipolar relaxation phenomena in the depolarization periods. This baseline is subtracted to analyze mainly the effects of light irradiation on samples charged with different polarities.

Figure 11 shows the results of the PSD measurements for both the scan mode and the fixed wavelength acquisitions. In the PSD current spectrum of Fig. 11 (a), several events can be seen in the UV region from which two current peaks stand out (negative peaks, consistently with the depolarization current): a very narrow one located at 360 nm and a slightly wider one located at 207 nm. The first peak is associated with an energy of 3.4 eV and appears only after the sample has been charged with fields higher than 120 kV/mm. The second peak appears in a higher energy region (5.9 eV) and is present in every pre-charged recording. The evolution of both peaks is different from each other, the one at 360 nm shows almost a tenfold increase in amplitude from PSD120 to PSD200 compared to the higher energy peak which evidence a first 12x growth from PSD40 to PSD120 followed by 46% raise until PSD200.

The current transient displayed in Fig 11 (b) and recorded during monochromatic irradiation at 215 nm shows that charge flow occurs with constant energy irradiations and that the transients behave differently depending on the previous applied field. In fact, one can observe that the higher the polarization fields, the higher the current amplitude both in the first minutes and in the rest of the transient. These current discharges may be associated with the space charge decrease after PSD measurements shown in Fig. 10 (c) and Table 2. They can be explained by charge detrapping phenomena particularly at high fields. These transient currents induced by light have no obvious relation with the discharge current measured in the dark: The small segment of discharge current in the dark before irradiation shown in Fig. 11 (b) is almost zero since it was recorded about 90 min after the voltage was set to zero volts.

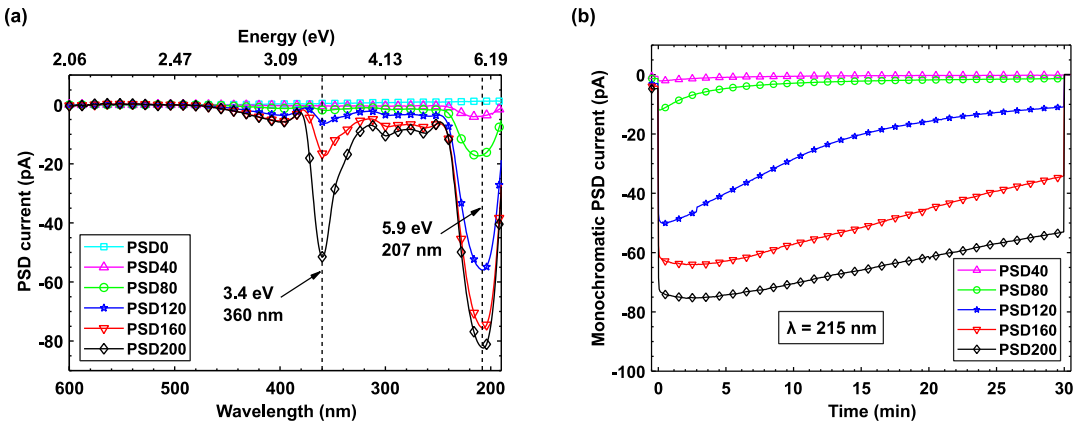

FIGURE 11. Photo-stimulated currents on a 12-µm thick PEN sample after being polarized under different electric fields. PSD spectra (a) and PSD transients at fixed wavelength (b).

DISCUSSION

Space charge density and photo-stimulated currents were studied on a PEN sample using a unique system combining LIMM and PSD techniques.

The sequential raw LIMM measurements show similar current spectra reflecting a stable state of charge within each six-acquisition interval. These signals allow to identify the presence of charge accumulation phenomena according to the magnitude and shape of their complex components. After signal processing, the residual electric field and the space charge density profiles are plotted as a function of the depth from the irradiated electrode. Unexpected behavior near the surface is related to the spatial diffusion of temperature, which is influenced by the laser penetration depth at the highest frequency and the numerical overshoot compensation.

The formation of a homocharge near the front electrode is verified, as well as charges of the opposite sign on the opposite side. Similar results have been reported on 25 μm and 50 μm thick PEN films using thermal and pressure wave stimuli methods [31–33]. The reproducibility of the results obtained through LIMM measurements demonstrate the robustness of the experimental setup. Additionally, the LIMM method proves to be more sensitive at shallow depths from the irradiated electrode. Even if the residual electric field caused by the space charge constitutes about 5% of the applied field, it can still be sensed by the test bench. LIMM measurements have clearly revealed the influence of light irradiation on the amount of trapped charges. The current signals related to the space charge are lower after perturbation by PSD measurements (both scan and fixed wavelength), a result that can demonstrate charge detrapping. The possibility of having information on the amount and localization of charges brings new opportunity to analyze light-induced mechanisms on polymers.

PSD spectra allow the identification of wavelength ranges promoting detrapping and macroscopic displacements of charge carriers. Two large peaks were found at 360 nm and 207 nm (3.4 eV and 5.9 eV respectively) along with non-negligible signals in the UV region. Although photocurrent spectra are sometimes normalized with the lamp emission characteristics[16,34] and can also be regularized with the absorbed energy per unit volume (irradiation dose), it is important to note that the signals presented in this study have not been corrected since the division of the current by the lamp photon flux density (Fig. 4) would disproportionately emphasize the high energy peak and hide the effects occurring across the entire UV spectrum. A further feature with using continuous scanning in wavelength for PSD acquisition is worth mentioning. During continuous scanning, not all of the trapped charges are released at an energy depth corresponding to the excitation wavelength. Therefore, it is expected that the detrapping of charges at depths lower than the excitation energy occurs, potentially leading to larger PSD currents in the high energy region of the continuous scanning than would be expected[35]. These observations point to irradiation dose and scanning speed effects on the obtained results. However, at the current stage of the research, the emphasis is primarily on the qualitative aspects of the spectra rather than quantitative analysis.

Electrode material play a significant role in both LIMM and PSD measurements considering the nature of the layer, its thermal and optical properties, as well as its shape. In LIMM acquisitions, the electrode that is subjected to laser beam heating must be able to transfer the greatest quantity of thermal energy to the sample. Therefore, materials with higher thermal capacity are preferred for this purpose. It has also been shown that the optical properties of the electrode material, such as the refractive index and the extinction coefficient, are essential for the accuracy of the implemented thermal model[36]. Investigations exploring the correlation between PSD outcomes and electrode material established that the photocurrent peaks can be associated to electron emission, as evidenced by the cutoff energy of the peaks aligning closely with the work function of the electrode material. For instance, results obtained with gold and aluminum electrodes on BOPP and PTFE films show photo-stimulated onset thresholds in the energy range corresponding to the respective metal work functions[16,37]. Moreover, the shape of the electrode is another critical factor to consider, as it can give rise to electric field enhancements resulting from the presence of electrode edges[37].

There are two primary motivations for employing thin samples in the coupled test bench. The first involves the LIMM method's capability to identify charge accumulation very close to the heated electrode. The second reason stems from the method's challenge in detecting charges as the sample depth increases, which can be attributed to the attenuation and dispersion of thermal waves. Hence, the sample thickness can be reduced to a point where the thermal zone generated by the laser remains consistent. In other words, the thickness should be greater than the zone of weak data precision while still allowing for the diffusion of thermal waves. Additionally, it is crucial to consider the characteristics of light absorption, as they determine the depth of light penetration. This parameter is closely associated with the effective irradiated zone within the sample, where interactions between photons and charges can take place. In this context, the current measuring setup enables the evaluation of numerous thin film polymers, particularly those commonly employed in film capacitors or flexible electronic devices.

CONCLUSION

A set up for simultaneous space charge density and photo-stimulated current measurements was implemented in a unique system combining LIMM and PSD techniques. Complete galvanic isolation is achieved by a controlled magnetic switch that allows the selection of one of the techniques depending on a predefined measurement program. As both methods involve very low amplitude current acquisitions, different noise reduction and signal processing strategies are applied to obtain both processible data and consistent results.

On a PEN film, light-induced current phenomena were directly related to changes in residual electric field and space charge profiles, particularly in the energy bands of 360 nm (3.4 eV) and 207 nm (5.9 eV), with secondary current peaks observed throughout the UV range.

The integration of LIMM and PSD methods within a shared test bench, and their sequential utilization in measurement programs, enables the monitoring of trap filling, the stimulation of trap release through UV-visible light irradiation, and the exploration of correlations between applied light energy and trap characteristics. Indeed, the measurement system demonstrates in an innovative approach that the reduction in space charge density after PSD measurements is directly attributed to the light disturbance itself, rather than being influenced by concurrent factors such time elapsed after charging or manipulations causing charge release.

The aforementioned test bench facilitates the transition to a subsequent phase of quantitative investigation into polymer thin films, providing the flexibility to modify various parameters. These include the protocols governing the applied electric field, the composition and thickness of the insulating material, the electrodes material, and their geometrical configuration.

Finally, the two techniques are shown to be complementary, but the analysis of the results remains complex because different phenomena are at play simultaneously. Additional experiments that allow the study of dielectric electronic transitions are required to distinguish the effects of each measured PSD peak on the space charge profiles.

AUTHOR DECLARATIONS

Conflict of Interest

The authors have no conflicts to disclose.

Author Contributions

Duvan Mendoza-Lopez: Data curation (lead); formal analysis (lead); methodology (equal); software (supporting); visualization (lead); writing – original draft (lead); writing – review & editing (equal). **Laurent Berquez**: Formal analysis (supporting); methodology (equal); software (lead); visualization (supporting); writing – review & editing (equal). **Laurent Boudou:** Formal analysis (supporting); methodology (equal); software (supporting); visualization (supporting); writing – review & editing (equal). **Gilbert Teyssedre:** Formal analysis (supporting); methodology (equal); visualization (supporting); writing – review & editing (equal).

DATA AVAILABILITY

The data that support the findings of this study are available from the corresponding author upon reasonable request.

REFERENCES

[1] J. Luo, J. Mao, W. Sun, S. Wang, L. Zhang, L. Tian, Y. Chen, and Y.H. Cheng, “Research Progress of All Organic Polymer Dielectrics for Energy Storage from the Classification of Organic Structures,” Macromol. Chem. Phys. **222**, (2021).

[2] O.G. Gnonhoue, A. Velazquez-Salazar, É. David, and I. Preda, “Review of Technologies and Materials Used in High-Voltage Film Capacitors,” Polymers **13**(5), 766 (2021).

[3] T.D. Huan, S. Boggs, G. Teyssedre, C. Laurent, M. Cakmak, S. Kumar, and R. Ramprasad, “Advanced polymeric dielectrics for high energy density applications,” Prog. Mater. Sci. **83**, 236–269 (2016).

[4] X. Li, Y. Wang, M. Xu, Y. Shi, H. Wang, X. Yang, Y. Haoting, and Q. Zhang, "Polymer electrets and their applications," J. Appl. Polym. Sci. **138**, 50406 (2020).
[5] V. Zardetto, T. Brown, A. Reale, and A. Di Carlo, "Substrates for Flexible Electronics: A Practical Investigation on the Electrical, Film Flexibility, Optical, Temperature, and Solvent Resistance Properties," J. Polym. Sci. Part B Polym. Phys. **49**, 638–648 (2011).
[6] G. Teyssedre, and C. Laurent, "Charge transport modeling in insulating polymers: from molecular to macroscopic scale," IEEE Trans. Dielectr. Electr. Insul. **12**(5), 857–875 (2005).
[7] M. Meunier, N. Quirke, and A. Aslanides, "Molecular modeling of electron traps in polymer insulators: Chemical defects and impurities," J. Chem. Phys. **115**(6), 2876–2881 (2001).
[8] G.C. Montanari, "Bringing an insulation to failure: the role of space charge," IEEE Trans. Dielectr. Electr. Insul. **18**(2), 339–364 (2011).
[9] A. Imburgia, R. Miceli, E.R. Sanseverino, P. Romano, and F. Viola, "Review of space charge measurement systems: acoustic, thermal and optical methods," IEEE Trans. Dielectr. Electr. Insul. **23**(5), 3126–3142 (2016).
[10] P. Notingher, S. Holé, L. Berquez, and G. Teyssedre, "An Insight into Space Charge Measurements," Int. J. Plasma Environ. Sci. Technol. **11**(1), 26–37 (2017).
[11] N. Belkahla, G. Teyssedre, N. Saidi-Amroun, M. Saidi, L. Boudou, and L. Berquez, "Space charge, conduction and photoluminescence measurements in gamma irradiated poly (ethylene-2,6-naphthalate)," Radiat. Phys. Chem. **101**, 73–80 (2014).
[12] G. Teyssedre, C. Laurent, L. Boudou, and S. Le Roy, in *2019 2nd Int. Conf. Electr. Mater. Power Equip. ICEMPE* (IEEE, Guangzhou, China, 2019), pp. 85–90.
[13] G. Teyssedre, F. Zheng, L. Boudou, and C. Laurent, "Charge trap spectroscopy in polymer dielectrics: a critical review," J. Phys. Appl. Phys. **54**(26), 263001 (2021).
[14] K. Kojima, Y. Takai, and M. Ieda, "Carrier Traps in Polyethylene Naphthalate (PEN): Photoelectret," Jpn. J. Appl. Phys. **21**(Part 1, No. 7), 1025–1027 (1982).
[15] J.C. Cañadas, J.A. Diego, J. Sellarès, M. Mudarra, J. Belana, R. Díaz-Calleja, and M.J. Sanchis, "Comparative study of amorphous and partially crystalline poly(ethylene-2,6-naphthalene dicarboxylate) by TSDC, DEA, DMA and DSC," Polymer **41**(8), 2899–2905 (2000).
[16] A. Mellinger, F.C. Gonzalez, and R. Gerhard-Multhaupt, "Photostimulated discharge in electret polymers: an alternative approach for investigating deep traps," IEEE Trans. Dielectr. Electr. Insul. **11**(2), 218–226 (2004).
[17] D. Mendoza-Lopez, G. Teyssedre, L. Berquez, and L. Boudou, in *2022 IEEE 4th Int. Conf. Dielectr. ICD* (2022), pp. 376–379.
[18] L. Boudou, F. Zheng, and G. Teyssedre, in *2018 12th Int. Conf. Prop. Appl. Dielectr. Mater. ICPADM* (2018), pp. 722–725.
[19] S.B. Lang, and D.K. Das-Gupta, "A technique for determining the polarization distribution in thin polymer electrets using periodic heating," Ferroelectrics **39**(1), 1249–1252 (1981).
[20] R. Singh, "A review of developments in thermal techniques for charge profile measurements in polymer electrets," J. Electrost. **72**(4), 322–329 (2014).
[21] G. Velarde, S. Pandya, J. Karthik, D. Pesquera, and L.W. Martin, "Pyroelectric thin films—Past, present, and future," APL Mater. **9**(1), 010702 (2021).
[22] A. Velazquez-Salazar, L. Berquez, and D. Marty-Dessus, "Thermal modeling and calibration in (F)LIMM using an external bias field: Theory and experiment," IEEE Trans. Dielectr. Electr. Insul. **25**(3), 783–790 (2018).
[23] A. Petre, D. Marty-Dessus, L. Berquez, and J.-L. Franceschi, "A Comparison of Different Mathematical Treatments for Solving the Inverse Problem in Focused Laser Intensity Modulation Method," Jpn. J. Appl. Phys. **43**(5R), 2572 (2004).
[24] A. Velazquez-Salazar, L. Berquez, and D. Marty-Dessus, in *2016 IEEE Int. Conf. Dielectr. ICD* (2016), pp. 223–226.
[25] J.D. Brodribb, D.M. Hughes, and T.J. Lewis, in *Electrets Charge Storage Transp. Dielectr.*, Perlman, M. (Dielectrics and Insulation Division, Electrochemical Society, 1973), pp. 177–187.
[26] F. Camacho González, Charge-Storage Mechanisms in Polymer Electrets, Ph.D. dissertation, Universität Potsdam, 2006.
[27] Keithley, *Low Level Measurements Handbook*, 7th Edition (Tektronix, n.d.).
[28] Keithley, *Model 617 Programmable Electrometer Instruction Manual* (Tektronix, 1988).
[29] R.J. Fleming, "Space charge profile measurement techniques: recent advances and future directions," IEEE Trans. Dielectr. Electr. Insul. **12**(5), 967–978 (2005).

[30] T. Pawlowski, R.J. Fleming, and S.B. Lang, "LIMM study of space charge in crosslinked polyethylene," IEEE Trans. Dielectr. Electr. Insul. **13**(5), 1023–1029 (2006).
[31] G. Teyssedre, L. Berquez, and C. Laurent, "Some aspects of coupled electrical-mechanical effects in dielectric materials," Eur. Phys. J. Appl. Phys. **70**(2), 20902 (2015).
[32] T.T. Anh, L. Berquez, L. Boudou, and J. Martinez-Vega, "Effect of trapped space charge on mechanical deformation induced by electric field," IEEE Trans. Dielectr. Electr. Insul. **18**(5), 1416–1422 (2011).
[33] J.L. Augé, G. Teyssedre, C. Laurent, T. Ditchi, and S. Holé, "Combined electroluminescence and charge profile measurements in poly(ethylene-2, 6-naphthalate) under a dc field," J. Phys. Appl. Phys. **33**(24), 3129–3138 (2000).
[34] L. He, Y. Chen, L. Dai, Y. Zhang, L. Zhao, J. Cao, X. Wang, and Q. Lei, in *2009 IEEE 9th Int. Conf. Prop. Appl. Dielectr. Mater.* (2009), pp. 1102–1105.
[35] Z. Zhu, Y. Zhang, Z. An, and F. Zheng, "Methodological investigation on photo-stimulated discharge to obtain accurate trap information in polymer dielectrics," Meas. Sci. Technol. **22**(8), 085109 (2011).
[36] F. Carrasco, K. Makasheva, D. Marty-Dessus, and L. Berquez, in *2021 IEEE Conf. Electr. Insul. Dielectr. Phenom. CEIDP* (IEEE, Vancouver, BC, Canada, 2021), pp. 627–630.
[37] P. Ma, Y. Zhang, S. Holé, F. Zheng, M. Gu, and Z. An, in *2016 IEEE Int. Conf. Dielectr. ICD* (2016), pp. 187–190.